Danmarks Tekniske Universitet

DTU

Assignment # 3
Turbulent flows

Authors

Marcos Garcia Bravo - s244059
Jakub Kuleta - s244053
Szczepan Zygmunt Letkiewicz - s244067

December 6, 2024

Contents

1 Introduction

This report showcases the procedure for analyzing flow measurement data of a free round jet. The air velocity signal captured by a single hot wire anemometer is subjected to statistical, correlational, and spectral analyses. This investigation primarily focuses on one out of the twelve measurement tests which were carried out, before considering the entire data set across different physical conditions. The flow is assumed to be isotropic through the study, which yields a special class of turbulence where statistical properties are invariant to rotation around the coordinate axis and imply homogeneous turbulence. This assumption is valid because the round jet is axisymmetric.

2 Measurement Data

Data from the hot wire anemometry consists of measured velocities at a distance of 20 diameters from the jet exit, for a range of exit velocities. In this report, sections up to section 6 analyse these measured velocities on test number 12, which has an exit velocity of 38.4 m/s. Firstly, consider the turbulent fluctuating velocity u' of the flow, as obtained from the decomposition $u' = u(t) - \overline{u}$. This fluctuating velocity is plotted as a time series in Figure 1, where the full experiment time of 10 s is shown in Figure 1a and a zoomed-in section of up to 0.03 s is shown in Figure 1b.

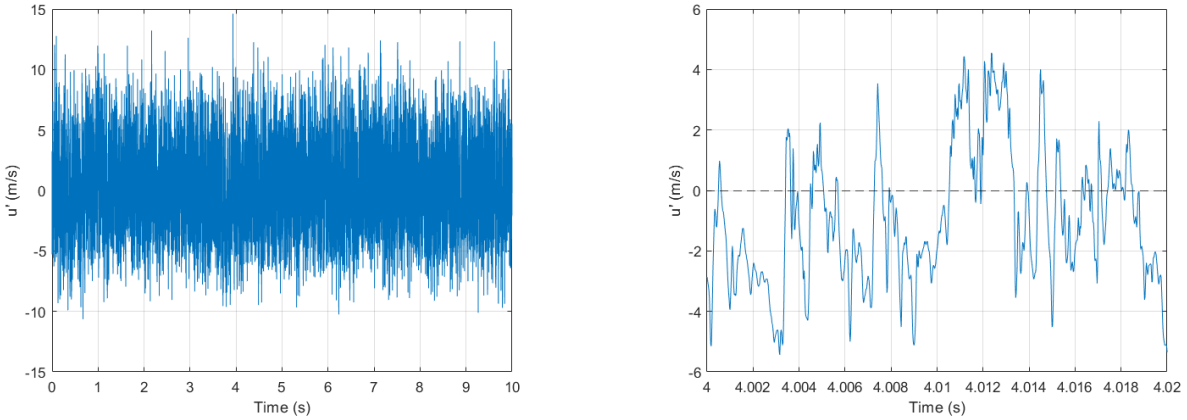

(a) Full experiment time series - 10 s.

(b) Zoomed in time series - 0.03 s.

Figure 1: Resultant turbulent fluctuating velocity as a function of time.

Individual eddies are not represented directly by the fluctuation peaks themselves. Instead, eddy structures in turbulence are coherent motions in the fluid. The peaks represent the instantaneous deviations of the velocity from the mean, hence a momentary fluctuation. On the other hand, eddy structures have length and time scales. The length scales of the eddies are seen in Figure 1b through the magnitude of u' deviating from zero for a given time range, representing the passing of an eddy through the measurement point.

3 Statistical Analysis

3.1 Basic Statistics

The basic statistics of the signal are shown in Table 1. The first central moment is the mean of the raw signal given by the following equation, where N is the number of measurements.

$$\bar{u} = \frac{1}{N}\sum_{i=1}^{N} u_i \tag{1}$$

The second central moment is the variance, which indicates the dispersion of the data. To determine the variance the standard deviation σ_u is used, as given by $\sigma_u = \sqrt{\overline{(u-\overline{u})^2}} = \sqrt{\overline{u'^2}}$. This means that the standard deviation is identical for both the fluctuating and mean velocity. Furthermore, it is also identical to the RMS value of the velocity.

$$\sigma_u^2 = \frac{1}{N}\sum_{i=1}^{N}(u_i - \bar{u})^2 \tag{2}$$

The third central moment is the skewness which indicates the asymmetry of a probability distribution around the mean. It is defined as follows:

$$S_u = \frac{1}{N\sigma_u^3}\sum_{i=1}^{N}(u_i - \bar{u})^3 \tag{3}$$

Lastly, kurtosis is the fourth central moment and depicts how extreme the values in the tails are compared to a normal distribution, which is defined as follows:

$$F_u = \frac{1}{N\sigma_u^4}\sum_{i=1}^{N}(u_i - \bar{u})^4 \tag{4}$$

Statistical parameters	Value
Mean $\overline{u}$	12.874 [m/s]
Standard deviation σ_u	3.106 [m/s]
Variance σ_u^2	9.648 [m^2/s^2]
Skewness S_u	0.089
Kurtosis F_u	2.848
Turbulence Intensity $\sigma_u/\overline{u}$	0.241

Table 1: Statistical parameters of the velocity field for test 12.

Table 1 also gives the turbulence intensity by $\sigma_u/\overline{u}$, which indicates the magnitude of velocity field fluctuations. Its value is 0.241, suggesting that it is rather small and thus the

frozen turbulence approximation can be used.

3.2 Probability density funtion

The probability density function $p(u')$ for the turbulent signal is shown in Figure 2, along with the normal distribution given by equation 5.

$$p(u') = \frac{1}{\sigma_u \sqrt{2\pi}} e^{\left(-\frac{u'^2}{2\sigma_u^2}\right)} \tag{5}$$

The normal distribution shows reasonable agreement with the experiment data. The peak of the probability density function occurs at the mean fluctuation velocity, 1.252×10^{-14} which can be assumed to be equal to zero.

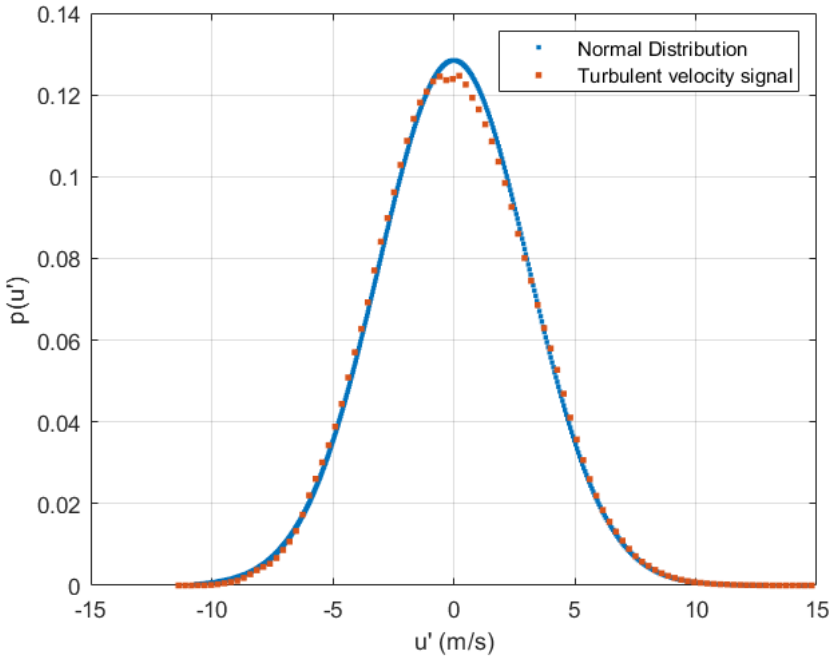

Figure 2: Probability density function for fluctuating velocity signal.

4 Correlation Analysis

4.1 Time correlation function

Eulerian time correlation describes how fluid flow properties evolve with time, using a reference fixed in space. The time correlation function R_E is computed discretly using equation 6, for each discrete time lag index while $R_E > 0$. Consider the result shown in Figure 3, where τ is the separation time between measurements.

$$R_E(\tau) = \frac{\overline{u'(\tau)u'(\tau+t)}}{\overline{u'^2}} \tag{6}$$

From equation 6, the Eulerian macro time scale T_E can be found by integrating $R_E(\tau)$ over the measured time. This represents the characteristic time it takes for a coherent structure of characteristic size Λ_f to pass the measurement point [1].

$$T_E = \int_0^\infty R_E(\tau)d\tau \tag{7}$$

Furthermore, the micro time scales τ_E are calculated by using the fact that $R_E(\tau = 0) = 1$ to determine the partial derivative in the definition[1]:

$$\tau_E = \left[-\frac{2}{(\partial^2 R_E(\tau)/\partial\tau^2)_{\tau=0}}\right]^{1/2} \tag{8}$$

Consider both time scales shown in Figure 3. By plotting the relation $R_e = e^{\left(-\frac{\tau}{T_E}\right)}$, against the time correlation obtained from equation 6, the time scales are verified.

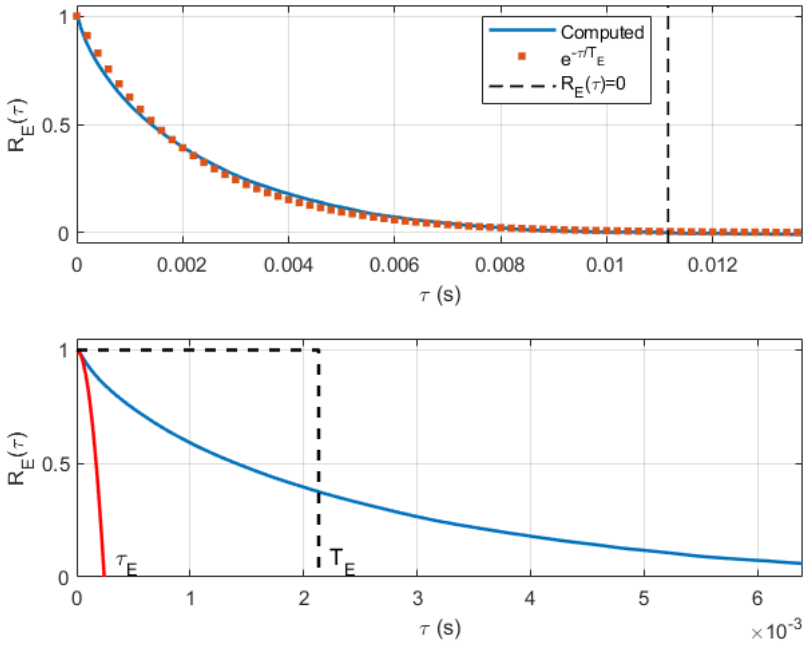

Figure 3: Eulerian time correlation plot

Figure 3 indicates that the macro time scale T_E is approximately 0.0021 s, which in comparison with Figure 1b corresponds to roughly one full cycle of fluctuations. This is

[1]The analogous micro time scale definition using turbulent velocity fluctuations can also be used $\tau_E = \sqrt{\frac{2\overline{u'^2}}{\overline{(\partial u'/\partial\tau)^2}}}$

equivalent to one coherent turbulent structure matching the definition of T_E, as illustrated in Figure 4.

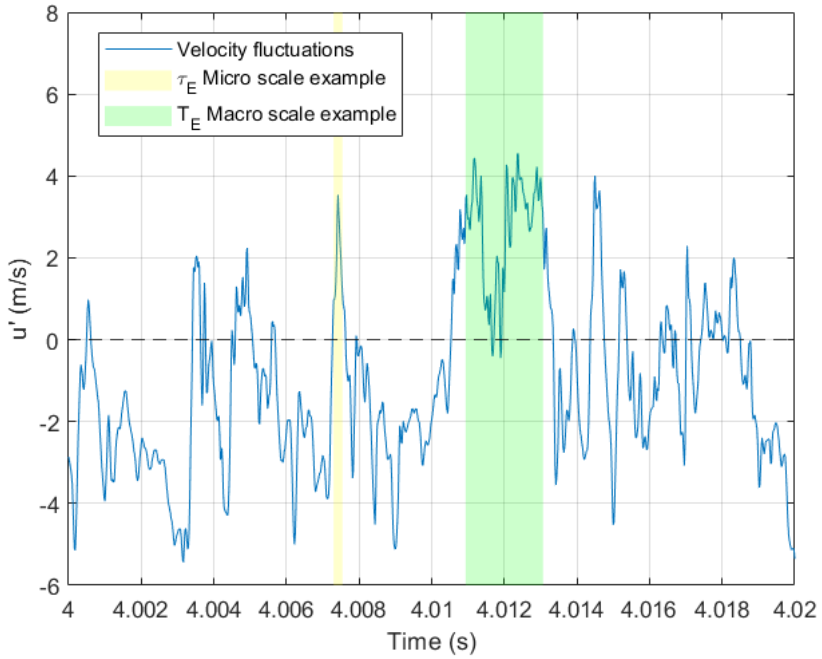

Figure 4: Resultant turbulent fluctuating velocity as a function of time with time scales.

4.2 Taylor's frozen turbulence Approximation

The frozen turbulence approximation states that the time and length scales are related. This relation is given by the following relations for macro and micro scales respectively.

$$\Lambda_f = \overline{u} T_E \tag{9}$$

$$\lambda_f = \overline{u} \tau_E \tag{10}$$

The corresponding calculated values are given in Table 2.

Taylor's frozen Approximation	Value
Micro Length Scale λ_f	0.0031 [m]
Macro Length Scale Λ_f	0.0276 [m]

Table 2: Approximations and their corresponding values.

For Taylor's frozen turbulence approximation to be valid on the macro scale, the turbulence intensity must be small i.e. $\sigma_u/\overline{u} << 1$. For the approximation to also be applicable

on the micro-scale, the viscous term must be negligible, which equates to having a large Reynolds number i.e. $Re_\lambda = \frac{\lambda \overline{u}}{\nu} >> 1$.

The turbulence intensity found in section 3 is 0.241, which means that Taylor's frozen turbulence approximation is valid for macro scales. The Reynolds number Re_λ is found to be 2665, also satisfying the condition for micro scales.

5 Spectral analysis

5.1 Kolmogorov Approximations scales

Kolmogorov's first hypothesis states that regardless of the large-scale motion, the universal equilibrium range is isotropic. Under these conditions, the dissipation rate ϵ can be expressed using the Taylor microscale corresponding to:

$$\epsilon = 30\nu \frac{\overline{u_1'^2}}{\lambda_f^2} \tag{11}$$

Based on a non-dimensional argument, the Kolmogorov length scale η_k and time scale τ_k are described by the following relations:

$$\eta_k = \left(\frac{\nu^3}{\epsilon}\right)^{1/4} \tag{12}$$

$$\tau_k = \left(\frac{\nu}{\epsilon}\right)^{1/2} \tag{13}$$

These relationships yield the estimated scales shown in Table 2.

Isotropic Turbulence Approximation	Value
Kolmogorov Time Scale τ_k	1.838×10^{-4} [s]
Kolmogorov Length Scale η_k	5.268×10^{-5} [m]
Disipation rate ϵ	447.068 [m^2/s^3]

Table 3: Approximations and their corresponding values.

5.2 Energy density spectra in frequency domain

The measurement data is analysed in the frequency domain using the energy spectrum, which is computed using the Fast Fourier Transform (FFT) and the Welch method. FFT computes the discrete Fourier transform of the entire sequence, whereas the Welch method, before carrying out discrete Fourier transform of the signal, it divides the sequence into overlapping segments, computes respective periodograms and takes average of them in order to remove noise. The energy spectrum is presented in Figure 5.

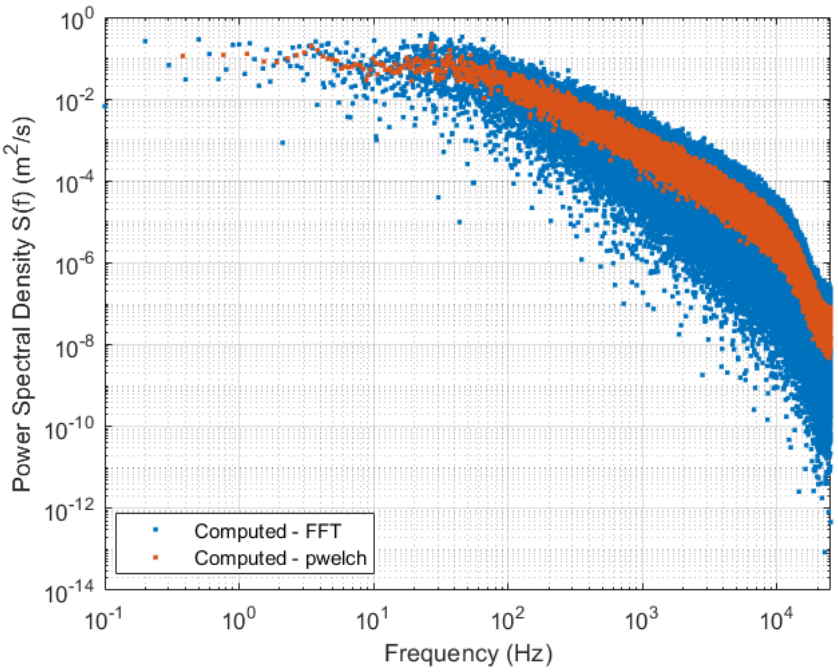

Figure 5: Energy spectrum of the measured flow using FFT and pwlech.

Figure 5 shows how the unsteady flow changes in time. The distribution indicates that eddies with large amounts of kinetic energy occur less often, whereas small-scale structures have a higher frequency. This is known as the turbulent energy cascade, which can be approximated by the decay $S(f) \sim f^{-5/3}$ in the inertial range.

To verify the calculation, the integral of the energy spectrum is taken to confirm that it is equal to the variance. The integral calculates the area under the curve, which corresponds to the variance according to Parseval's theorem shown in equation 14.

$$\sigma_u^2 = \frac{1}{T}\int_0^T |u(t)|^2 \, dt = \int_0^\infty S(f)_{FFT} \, df = 9.648 \; [\mathrm{m}^2/\mathrm{s}^2] \tag{14}$$

The integral of the energy spectrum computed using the Welch method yields 9.5784, which is slightly lower than the variance. The reason for this difference is the averaging process used by the method to remove some of the noise.

5.3 Energy density spectra in wave number space

The energy spectrum can also be expressed in terms of wave number k, through the relation $k = 2\pi f/\overline{u}$. Using Taylor's frozen approximation, which was proven to be applicable for this flow case in section 4, the one-dimensional model wave number spectrum $F(k)$ is given by equation 15.

$$F(k) = \frac{1}{2}\frac{\overline{u}}{2\pi}S(f) \tag{15}$$

Based on Kolmogorov's $-5/3$ law, the relation $F(k) \sim k^{-5/3}$ can be modelled by the von Karman spectrum defined by equation 16.

$$F(k) = \frac{\Lambda_f \overline{u'^2}}{\pi} \frac{1}{\left[1 + 70.78 \left(\frac{k\Lambda_f}{w\pi}\right)^2\right]^{5/6}} \tag{16}$$

Consider the one-dimensional energy spectra in terms of the wave number in Figure 6, which shows two methods of computing, FFT and Welch method, the von Karman model and a $-5/3$ slope for reference. Since this spectra captures turbulence, a 3D phenomenon, in 1D there is likely a misrepresentation error known as aliasing.

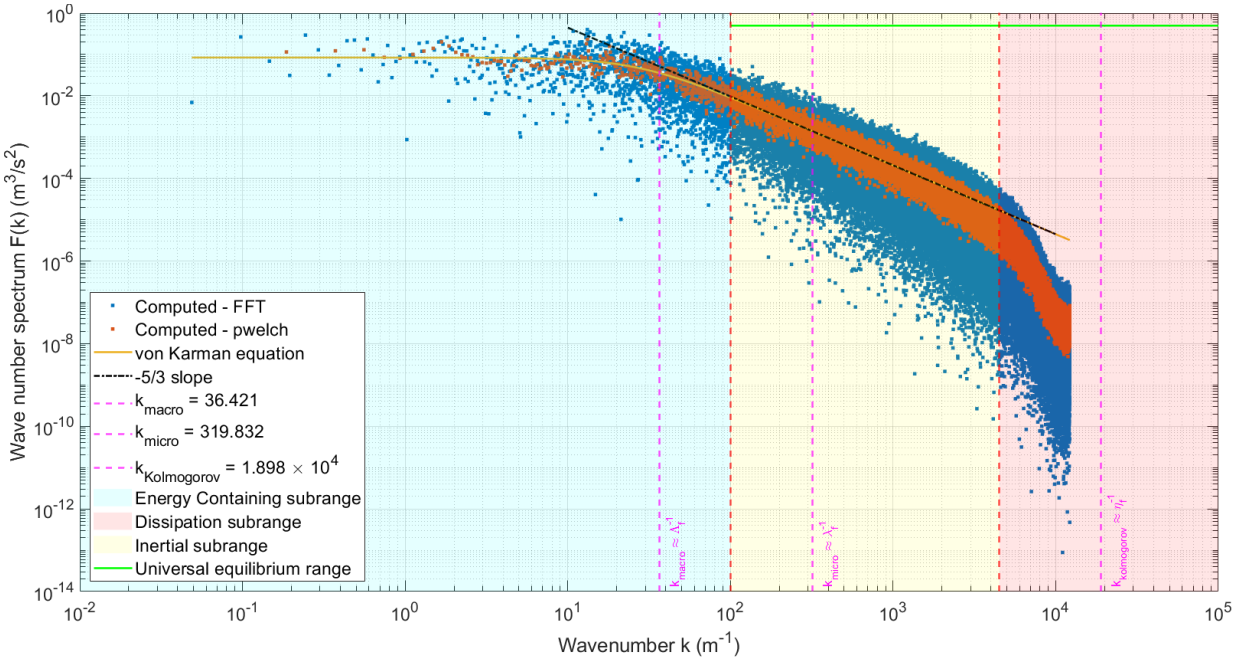

Figure 6: One-dimensional energy spectra in terms of the wave number.

The spectrum is identical to the energy spectrum in terms of frequency because wavenumber k and frequency f are equivalent. To verify the spectra's validity, the integral of the spectrum must yield half of the variance, because of the 1/2 factor in equation 15. This validation is presented in equation 17.

$$\sigma_u^2 = 2 \int_0^\infty F(k)_{FFT}\, dk = 9.648\ [\mathrm{m}^2/\mathrm{s}^2] \tag{17}$$

5.3.1 Energy cascade ranges

The energy cascade consists of the universal equilibrium range and three subranges. The universal equilibrium range starts at the point where the initial large-scale motion does not influence the energy transfer, hence it is independent of the flow environment. This is

presented in Figure 15 by the green line, showing where the flow is isotropic and the energy thus depends on the following quantities: $E = f(\epsilon, \nu, k)$. Kolmogorov's first hypothesis predicts that this range starts where the energy spectra resembles the trendline $-5/3$.

Consider the following description of the subranges which correspond to Figure 15.

- **Energy Containing Subrange:** refers to the range of large-scale structures, where most of the kinetic energy is concentrated. This range is found at low wavenumbers k.
- **Inertial Subrange:** region where energy is transferred from large-scale to small-scale eddies following the Kolmogorov $-5/3$ law. This subrange is part of the universal equilibrium range and is independent of viscosity, as no significant dissipation occurs.
- **Dissipation Subrange:** indicates the smallest scale structures where kinetic energy is dissipated into heat due to viscous effects. It states at the point when the Kolmogorov law no longer holds.

5.3.2 Characteristic length scales

Taking the inverse of the previously calculated characteristic length scales expresses the scales in terms of wavenumber k, such that they can be plotted in Figure 15. Firstly, the macro length scale $\Lambda_f^{-1} \sim k_{macro}$ falls under the Energy-containing subregion. The macro length scale corresponds to large structures, which occur in this subrange. Secondly, the micro length scale $\lambda_f^{-1} \sim k_{micro}$ falls into the inertial subrange. This scale is interpreted as the size of small scales, which is why it correctly corresponds to this range. Lastly, the $\eta_k^{-1} \sim k_{Kolmogorov}$ is located in the dissipation subrange, past all the plotted data points. This length scale represents the scale of structures before they dissipate into heat, meaning that they are so small that the measured data does not capture it.

6 Full Data set

The length scales are computed for the remaining measurement tests using the same approach shown for test 12 in sections 4 and 5. Expressing the micro and Kolmogorov scales as a ratio of macro length scale Λ_f allows for a comparison with Reynolds number, as shown in Figure 7.

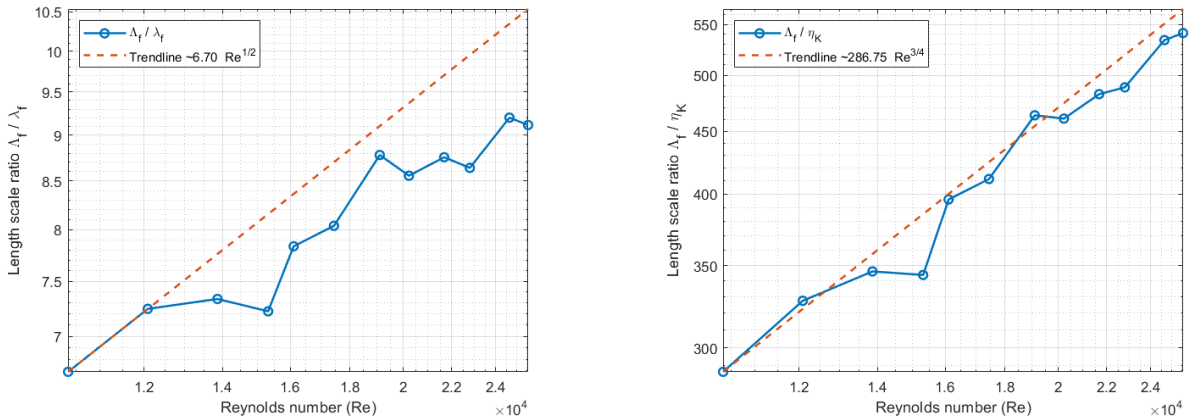

(a) Micro scales λ_f (b) Kolmogorov scales η_k

Figure 7: Length scales as a function of Reynolds number for tests 1-12.

Based on Figure 7a it can be seen that flow follows the trend of $Re^{1/2}$ for the micro-scale. On the other hand, the Kolmogorov scale slightly differs from the predicted trendline of $Re^{3/4}$, but does suggest a similar behaviour. This implies that the large and small scales in a turbulent flow like this one will become more widely separated as the Reynolds number is increased.

7 Conclusion

To conclude, this report has detailed turbulent flow data's statistical, correlation, and spectral analyses, focusing on a round jet experiment. The study confirmed the validity of Taylor's frozen turbulence approximation, with both macro and micro scales satisfying the necessary conditions. Statistical parameters revealed a low turbulence intensity, while probability density functions and correlation analysis provided insight into velocity fluctuations and temporal evolution. Spectral analysis validated Kolmogorov's -5/3 law in the inertial range, highlighting the energy transfer across scales and the separation of large and small-scale structures with increasing Reynolds numbers. These findings contribute to a deeper understanding of turbulent flow dynamics and scaling behaviours, providing insight into the structures present in the flow.

List of Figures

References

[1] B. M. Sumer and D. R. Fuhrman, *Turbulence in Coastal and Civil Engineering*. Advanced Series on Ocean Engineering, World Scientific, 2020.